

The response of porous Al₂O₃ probed to nanoindentation

Zhong Ling^{a,*}, Xiaolin Wang^b, Jan Ma^c

^a LNM, Institute of Mechanics, Chinese Academy of Sciences, Beijing 100080, PR China

^b Institute of Acoustics, Chinese Academy of Sciences, Beijing 100080, PR China

^c School of MSE, Nanyang Technological University, Singapore 639798, Singapore

Received 6 June 2006; received in revised form 16 October 2006; accepted 26 October 2006

Abstract

The response of porous Al₂O₃ to nanoindentation was investigated at microscopic scales (nm– μ m) and under ultra-low loads from 5 to 90 mN with special attention paid to the dependence of the load–depth behaviour to sample porosity. It was found that the load–depth curves manifest local responses typical of the various porous structures investigated. This is particularly clear for the residual deformation after load removal. Similarly, the limited mean pressure of the sample containing small grains and interconnected pores is consistent with its porous structure. By comparison, the samples with larger grain size and various porous structures exhibit higher pressures and smaller residual deformations that can be attributed to the mechanical response of the solid phase.

© 2007 Elsevier B.V. All rights reserved.

Keywords: Porous Al₂O₃; Microstructure; Mechanical response; Nanoindentation

1. Introduction

Porous Al₂O₃ has received wide attention because of its functional applications resulting directly from its porous structure, such as high surface area, low density and increased specific strain at failure [1]. The mechanical reliability of porous ceramics depends on pore geometry, grain arrangement in the solid phase and on the bonding strength. It is known, in effect, that the grain bonding area and bounding strength dominate the mechanical properties of porous ceramics [2–8]. Wang [2] and Rice [3] deduced that the porosity and the porous patterns of porous ceramics would act on the Young modulus of the material. Green et al. [4] emphasized that grain bonding and the resultant porous structure should affect certain properties of porous ceramics. Recently, Deng et al. [5] indicated that the macroscopic mechanical properties of some porous alumina could be improved, but there is no support for this from microscopic tests. Whereas models for the mechanical behaviour of porous ceramics [1] are available, certain important parameters such as the porous frame, grain bonding and bonding strength, remain to be determined by microscopic tests [6–8].

The nanoindentation technique was developed as an effective tool for probing mechanical properties of dense materials at very small scales with high precision [9,10]. The micro-response of porous materials has recently been investigated by this technique [11–14]. It was applied in the present investigation to probe porous Al₂O₃ with various grain sizes and microstructures at microscales (nm– μ m) and ultra-low loads (mN).

2. Experimental procedure

2.1. Samples and microscopic tests

Porous Al₂O₃ was fabricated by pressing various size powders then sintered to the desired 85% theoretical density (T.D.). Sample I was made from nano-grains of α -Al₂O₃ with a starting size of 50 nm sintered in air at 1550 °C for 2 h. Sample II was fabricated with fine pure α -Al₂O₃ (TM-DAR, particle size range 0.1–0.3 μ m, surface area 13.6 m² g⁻¹, Taimei Chemical Co. Nagano, Japan), and sintered in air at 1250 °C for 10 min. Sample III was made with alumina powders (AKP50, particle size range 0.1–0.3 μ m, surface area 9–16 m² g⁻¹, Sumitomo Chemical Co., Osaka, Japan) and sintered as for sample II. The density, porosity and grain size of each sample are shown in Table 1. The densities of the samples were measured by physical measurement of the mass and volume (from diameter and

* Corresponding author. Tel.: +86 10 62545533x2048; fax: +86 10 62579511.
E-mail address: lingz@lnm.imech.ac.cn (Z. Ling).

Table 1
Main parameters and mechanical data ($P = 10$ and 90 mN) of the tested porous alumina samples^a

Sample	Porosity	Grain size (nm)	h_m (nm)		ε_{re} (%)		$(h_m - h_f)/h_m$ (%)		p (GPa)	
			h_{10}	h_{90}	ε_{10}	ε_{90}	$P = 10$ mN	$P = 90$ mN	p_{10}	p_{90}
I (α -Al ₂ O ₃)	0.193	100–300	460	1300	80	80	24	15	3.1	3.4
II (TM-DAR)	0.19	200–500	187	540	57	60	57	35	20.7	24.4
III (AKP50)	0.16	200–900	147	449	46	53	62	46	25.6	37.1

^a h_m , ε_{re} , $(h_m - h_f)/h_m$ and p are the maximum depth at a peak load, the residual deformation after unloading, the strain recovered after unloading and mean pressure over an indent, respectively.

thickness values) of the disk samples. Grain sizes were measured by scanning electron microscopy (SEM) examination of the cross-section of the samples and 200 grains were used (ASTM standard E112). The morphology of the pores of each porous Al₂O₃ sample was characterized on freshly fractured surfaces in a high-resolution scanning electron microscopy system (SEM Sirion400NC).

Nanoindentation tests were performed at room temperature with a fully calibrated [9] nanoindenter (CSEM Instrument) equipped with a Berkovich tip (3-face pyramid). The peak load levels were preset at 5, 10, 30, 50, 70 and 90 mN and the loading rate over the peak load was 2 min^{-1} ($[\Delta P/P] \text{ min}^{-1}$). The samples were finely diamond-polished till a scratch-free surface was obtained. In each test, the indenter was driven at the above-indicated rate into the specimen till the load reached the preset peak load level and then unloaded gradually to zero. For each peak load, five tests were conducted at different locations in a sample. The resultant indentations were observed by atomic force microscopy (AFM).

2.2. Analysis method

The real response of the deformation region around the nanoindent could be obtained based on the load levels, P (mN), against the tip depth, h (nm). The mean pressure is defined by, $p = P(h)/A(h)$, where $A(h)$ is the projected area of the indent [1], obtained by the standard calibration procedure [9] as

$$A = 24.56h_c^2 + C_1h_c^1 + C_2h_c^{1/2} + \dots + C_8h_c^{1/128} \quad (1)$$

where h_c is the contact depth of the indent. It is, however, noted that h_c and Eq. (1) is defined for dense and homogenous materials [9]. In Eq. (1), the indent tip radius and surface roughness, as well as the load frame compliance during indentation, have all been taken into account, especially at shallow depths. The residual deformation ε_{re} after unloading is defined by:

$$\varepsilon_{re} = \frac{h_f}{h_m} \quad (2)$$

where h_f is the residual depth after unloading, and h_m is the maximum depth at the peak load level. Both h_f and h_m can be obtained experimentally.

3. Results and discussion

3.1. Microscopic characterization

SEM images of the fracture surfaces of each sample are presented in Fig. 1. Fig. 1a shows the pore structure of sample I whose grain size is about 100–300 nm. The porous structure is comprised of assembled grains with few large, interconnected voids. The grain size of sample II (Fig. 1b) is about 200–500 nm and, by contrast with sample I, the porous structure consists of few small isolated voids. Fig. 1c is representative of the fracture surface of sample III. The grain size, about 200–900 nm and larger than the starting grain size, is also larger than that of sample II. The pores are either connected or isolated, however, in a way different from what is observed in the other two samples (Fig. 1c).

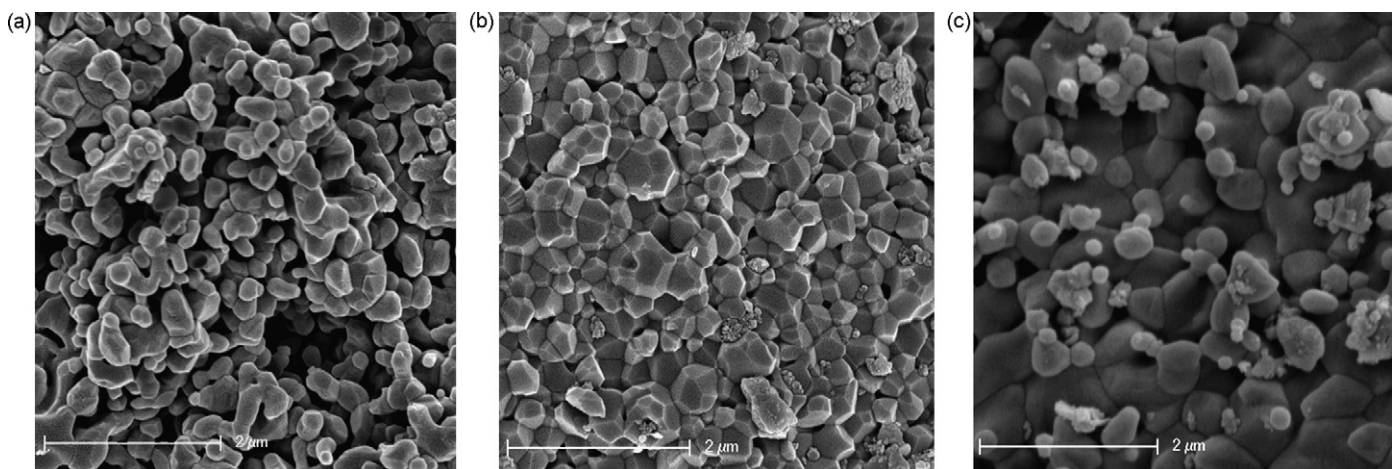


Fig. 1. SEM images of the fracture surfaces. (a) Sample I, grain size of 100–300 nm; (b) sample II, grain size of 200–500 nm; (c) sample III, grain size of 200–900 nm.

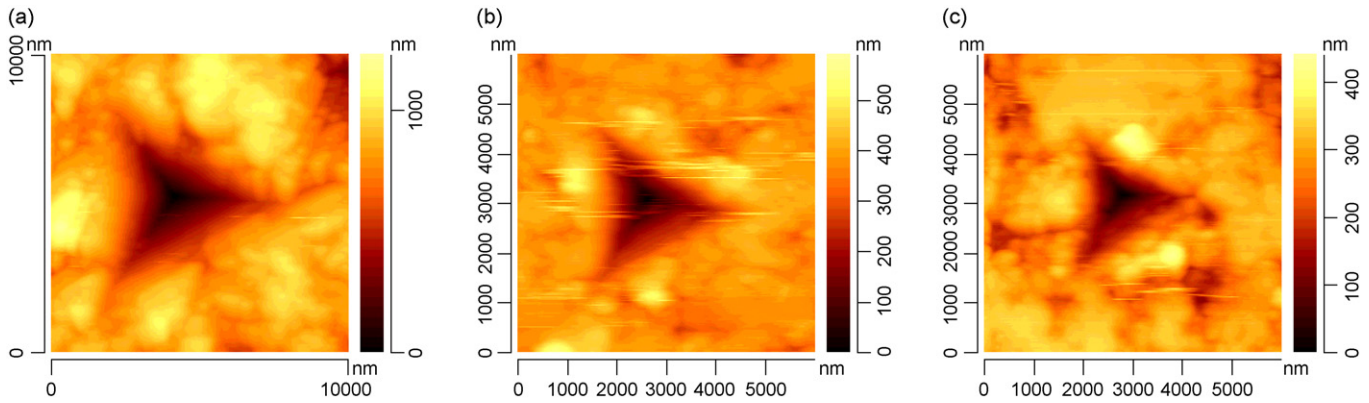


Fig. 2. AFM images of the indents under peak load of 90 mN. (a) Sample I; (b) sample II; (c) sample III.

AFM images of resultant indents under a peak load of 90 mN are showed in Fig. 2. The residual depths are about 1000, 500 and 400 nm for samples I, II and III, respectively.

3.2. Loading–unloading curves

Fig. 3 shows the load–depth curves recorded at three different locations on sample I under a maximum load of 10 mN. The loading tracks, which exhibit a few pop-ins, are different from each other with maximum indenter depths of 348, 444 and 570 nm, respectively. There is no pop-in event in the unloading part. The final depths of these indentations after unloading are of 265, 365 and 482 nm, respectively.

Fig. 4 displays the normalized load response, P/P_{max} , against the normalized depth, h/h_{max} , of all the samples submitted to the same peak load, 10 mN. The response of sample I to loading–unloading differs from those of samples II and III. In particular, there is no pop-in in the loading parts for the latter two samples. The residual deformations are such that $(\epsilon_{re})_I > (\epsilon_{re})_{II} > (\epsilon_{re})_{III}$.

Fig. 5 is a plot of the average maximum depths under peak loads for all three samples. Given a peak load, the tip penetrations in sample I display the largest scatter, in consistency with the variations of the tip penetrations h_m and h_f of sample I shown

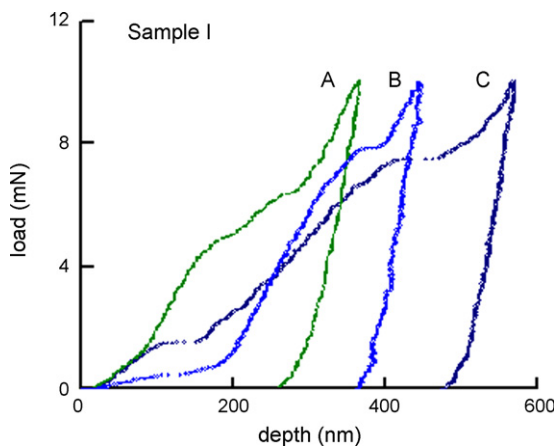


Fig. 3. Load vs. penetration depth at three locations of sample I, $P_m = 10$ mN.

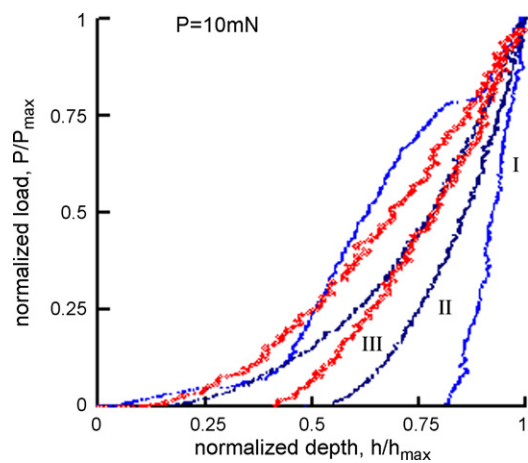


Fig. 4. Normalized responses, $P/P_m \sim h/h_m$, $P_m = 10$ mN.

in Fig. 3. The tip penetration is also the greatest of all in sample I, sample I “is the softest”.

3.3. Mean pressure and deformation

Fig. 6 plots the mean pressures p (Section 2.2) against the maximum indentation depth for the three samples. In sam-

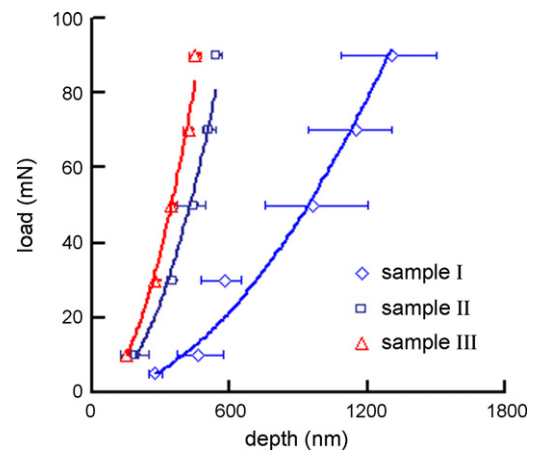


Fig. 5. Load vs. penetration depth in the tested samples, $P_m = 5–90$ mN.

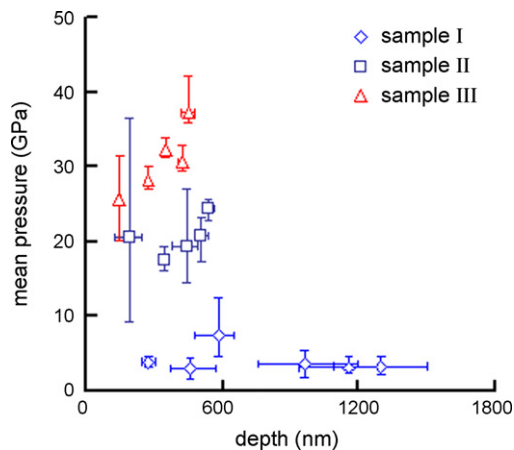


Fig. 6. Mean pressure vs. penetration depth, $P_m = 5\text{--}90\text{ mN}$. The penetration depths display conspicuous scatters in sample I, whereas for samples II and III the scatter on the mean pressure is more pronounced than that on the depth.

ple I, p lies between 3 and 7 GPa for a penetration range of 300–1600 nm. The mean pressure for sample II is about 10–25 GPa and this corresponds to penetration depths between 200 and 550 nm. The mean pressure is the largest with sample III, amounting to 20–38 GPa for a penetration range limited to 150–450 nm.

In Table 1, the data in the two columns for h_m , ε_{re} , $(h_m - h_f)/h_m$ (the strain recovered after unloading) and p are averaged values measured under $P = 10\text{ mN}$ and $P = 90\text{ mN}$, respectively. The maximum depth h_m and the residual deformation ε_{re} of sample I are greater than those of samples II and III. On the other hand, the mean pressures of sample I are almost load independent and much lower than those of samples II and III whose mean pressures increase with peak load.

3.4. Discussion

As presented in the foregoing sections, with its larger scatters in tip depth and with its higher residual deformation, sample I is “soft”, exhibiting by far the lowest mean pressures (Figs. 5 and 6). The pop-in occurring during the loading (Fig. 3) is caused by the local response of the microstructure, such as indentation on pores or grain collapse. When the indenter tip touches the solid phase, the solid phase resists the tip, so that only the load on the tip increases. In the case there is a pore or else grains beneath the tip are collapsing, there is no resistance at all from the solid phase. Accordingly, the depth of the tip keeps increasing at a constant load. These curves exhibit pop-in events accompanied by an increase in the indentation depth. As the load is increased, the indenter tip runs deeper into the sample touching larger parts of the solid phase while more grains may concomitantly collapse. Thus, increasing the load leads to a larger dispersion of the penetration depth (Fig. 5). Moreover, the fact that the pressure is limited even for high loads (Fig. 6) indicates that the mean pressure is determined by the weak elements of the sample microstructure. It is worth noting that the present indenter tip radius is 50–100 nm, thus approaching the grain size of sample I, and much smaller than the maximum depth

of penetrations (Table 1). Hence, the fact that the mean pressure is limited inspite of large indenter penetrations is attributed to local responses involving fracture events of the porous cells, or grain collapse [1,12]. In other words, it is the porous structure and its weak strength that make sample I “the softest” (Fig. 5).

On the other hand, the mean pressures of the large-grained samples display very prominent scatters (Fig. 6) which, we believe, are caused by the special porous structures of these samples (Fig. 1b and c). The indenter tip radius is again much smaller than the grain size (Table 1). As analyzed before, the indenter tip is opposed by the solid phase comprised of larger grains. The larger the grains, the smaller the deformation, hence, the higher the resistance to the tip. The maximum penetration depths in samples II and III are 450–550 nm, i.e. within the grain size range of 200–900 nm. The higher mean pressures against shallower penetration and lower residual deformation are consistent with a reaction dominated by the solid phase.

4. Conclusions

- (i) Under given peak loads, sample I with its relatively small grains and porous structure formed of interconnected pores, exhibits low mean pressures and deep penetration. The limited mean pressure is ascribed to the porous structure, while the larger depth and the dispersion of the indentation depth are believed to be caused by either the indentation of pores or by grain collapse.
- (ii) Under the same load range, samples II and III, which contain relatively large grains and a porous structure unlike that of the sample I, present higher mean pressures and shallower associated penetration. The higher pressures and their substantial scatter together with small residual deformations originate from the response of the solid phase.

Acknowledgements

This work is financially supported by National Natural Science Foundation of China (Grant No. 50172053, 10472120) and Chinese Academy of Sciences (Grant No. KJCX2-SW-L2 and KJCX2-YW-M04).

References

- [1] L.J. Gibson, M.F. Ashby, Cellular Solids: Structure and Properties, second ed., Cambridge Press, 1997.
- [2] J.C. Wang, J. Mater. Sci. 19 (1984) 801–814.
- [3] R.W. Rice, J. Am. Ceram. Soc. 76 (7) (1993) 1801–1808.
- [4] D.J. Green, et al., J. Am. Ceram. Soc. 78 (1) (1995) 266–268.
- [5] Z.Y. Deng, et al., J. Am. Ceram. Soc. 84 (11) (2001) 238–244.
- [6] C.D. Dam, et al., J. Mater. Res. 5 (1) (1990) 163–171.
- [7] A.P. Roberts, E.J. Garboczi, J. Am. Ceram. Soc. 83 (12) (2000) 3041–3048.
- [8] C.E. Wen, et al., Mater. Lett. 58 (2004) 357–360.
- [9] W.C. Oliver, G.M. Pharr, J. Mater. Res. 7 (6) (1992) 1564–1583.
- [10] B. Yang, H. Vehoff, Mater. Sci. Eng. A 400–401 (2005) 467–470.
- [11] A.G. Alcal, et al., Nanotechnology 13 (2002) 451–455.
- [12] Y. Toivola, et al., J. Mater. Res. 19 (1) (2004) 260–271.
- [13] L. Shen, K.Y. Zeng, Microelectron. Eng. 71 (2004) 221–228.
- [14] Z. Xia, et al., Acta Mater. 52 (2004) 931–944.